Materials and Structures (2020)53:94
https://doi.org/10.1617/s11527-020-01529-1

ORIGINAL ARTICLE

Experimental procedures for the mechanical characterization of composite reinforced mortar (CRM) systems for retrofitting of masonry structures

Tommaso D'Antino · Angelo Savio Calabrese · Carlo Poggi

Received: 28 March 2020 / Accepted: 6 July 2020

Abstract Fiber-reinforced composites can be arranged in the form of bi-dimensional grids and employed as internal reinforcement of mortar plasters to realize composite reinforced mortar (CRM) systems. Recently, CRM were applied as externally bonded reinforcement of existing masonry members showing promising improvements of load-carrying and deformation capacities. However, since CRM systems are still in their infancy, limited research is available regarding their mechanical properties and their bond behavior with respect to masonry substrates. In this paper, a series of experimental tests are performed on a CRM system comprising a glass fiber-reinforced composite grid and a lime-based matrix. Namely, tensile tests of bare grid yarns and of CRM coupons, shear tests of grid joints, and single-lap direct shear tests of CRM-masonry joints were performed. These tests are aimed at providing a comprehensive mechanical characterization of the CRM, which results can be used to design strengthening applications with this system. Namely, the tensile properties of bare grid yarns in warp and weft direction are obtained and compared with those of CRM coupons tested following the indications of the Italian and U.S. acceptance criteria for inorganic-matrix composites. Furthermore, the grid joints are subjected to shear tests to determine if the yarns orthogonal to the applied load direction provide a contribution to the system load-carrying capacity. Finally, CRM-masonry joints are subjected to single-lap direct shear tests to study the CRM bond behavior. This work provides an insight on the behavior of CRM that can be useful to formulate reliable design procedures for these systems.

Keywords Composite reinforced mortar (CRM) · FRCM · TRM · Tensile tests · Bond tests

1 Introduction

The growing need of retrofitting existing masonry structures to preserve or extend their service life has been fostering the research of innovative and effective strengthening solutions. Among them, fiber-reinforced polymer (FRP) composites have been largely adopted as externally bonded reinforcement (EBR) to increase the load-carrying capacity of masonry members subjected to various loading configurations [1–6]. However, due to the use of polymer (organic) adhesives, FRP composites have low compatibility with masonry substrates and are hard to remove [7]. To overcome these issues, the organic resin can be replaced by inorganic binders and the continuum fiber sheet by open-mesh textiles to form inorganic-matrix

T. D'Antino (✉) · A. S. Calabrese · C. Poggi
Department of Architecture, Built Environment and Construction Engineering, Politecnico di Milano, Piazza Leonardo da Vinci 32, 20133 Milan, Italy
e-mail: tommaso.dantino@polimi.it

Published online: 16 July 2020

composites usually referred to as fiber-reinforced cementitious matrix (FRCM) composites [8]. In FRCM composites, the inorganic matrix provides vapor permeability, protects the embedded textile from UV ray exposure, and is responsible for the stress-transfer mechanism between the composite and the substrate [9–11]. The reinforcing textiles can be made by various high-strength fibers, such as carbon, glass, basalt, polyparaphenylene benzobisoxazole (PBO), and steel, whereas cement-based, lime-based, and geopolymer matrices can be employed [12]. Organic coatings can be applied to the fiber textiles to improve the adhesion with the inorganic matrix and improve the fiber durability. FRCM composites were proven to be effective in increasing the load-carrying capacity of masonry arches [13], masonry columns [14, 15], and of masonry panels subjected to in-plane [16] and out-of-plane [17] loads. However, the use of high-strength textiles and (sometimes) of high-performance matrices, as well as the need of careful alignment of the reinforcing textile, are responsible for the relatively high price of this strengthening solution.

Recently, a newly-developed externally bonded strengthening solution comprised of fiber-reinforced composite grids embedded within an inorganic mortar has been developed [18–20]. These systems, referred to as composite reinforced mortar (CRM) [21], can be applied by simply fixing the composite grid to the masonry surface using anchors and then spraying the mortar over it. The rapidity of this procedure, which does not require the careful alignment of the fiber textile as in the case of FRCM composites, makes CRM an attractive and cost-effective solution for strengthening masonry structures. In general, the composite grids used in CRM are made by glass fibers fully impregnated with epoxy resin to form a bi-dimensional rigid grid. The warp and weft yarns have a clear spacing equal to or higher than 30 mm, whereas the matrix thickness can go up to 50 mm [21].

Limited research is available regarding CRM systems, which makes the formulation of reliable design procedures a difficult task. Furthermore, indications to perform experimental tests for the characterization of the entire CRM system are missing. Recently, acceptance criteria for CRM systems were released in Italy [21]. These criteria focus on the mechanical properties of the composite grid rather than on the behavior of the strengthening system. Since the mortar is responsible for the stress-transfer mechanism between the externally bonded reinforcement and the substrate, it plays a fundamental role in the contribution of the CRM to the strengthened member load-carrying capacity. Therefore, a careful characterization of the system should include the behavior of the entire CRM, the study of its relationship with the specific substrate considered, and the effect of possible anchors.

The main goal of this paper is the definition of appropriate experimental tests of CRM systems and of their components to obtain the mechanical properties needed to design different CRM strengthening applications. Furthermore, indications concerning the set-up and instrumentations of each specific test procedure are provided. The following mechanical properties of the reinforcing system are considered:

- Mechanical properties of bare (i.e. not impregnated with the inorganic matrix) grid yarns and mortar;
- Shear strength of joints connecting grid warp and weft yarns;
- Tensile behavior of the CRM system, investigated by different tensile tests of CRM coupons;
- Bond behavior of the CRM system, determined using single-lap direct shear tests of CRM-masonry joints comprising historic bricks.

The procedure and results obtained provide important indications on the main mechanical properties of CRM systems and on the experimental procedures needed to obtain a full mechanical characterization of these strengthening materials.

2 Mechanical properties of grid yarns and mortar

In this paper, a commercial CRM system was studied. In this section, the mechanical properties of the fiber-reinforced composite grid and of the mortar are investigated. These properties are of fundamental importance to understand the stress-transfer mechanism between the externally bonded reinforcement and the substrate.

2.1 Composite grid

The yarns of the grid were comprised of alkali-resistant glass fibers impregnated with epoxy resin [22]. The composite grid was made by pultruded yarns

in weft (x) direction and laminated yarns in warp (y) direction weaved together using the leno weave technique. Accordingly, each warp yarn was comprised of two sub-yarns twisted together and around the weft yarns, which contributed to provide a relatively high stiffness to the grid. The warp and weft yarns were spaced at 40 mm on center, as shown in Fig. 1. The mechanical properties of the grid were investigated by tensile testing of single weft (7 tests) and warp (7 tests) yarns [20]. The fiber cross-sectional areas A_f of the single weft and warp yarns were determined according to CNR-DT 200 R1/13 [23] and are reported in Table 1. The fiber cross-sectional area of the warp yarn reported in Table 1 is the overall area of the yarn made by two sub-yarns. The fiber volume fraction of the weft yarns, which is defined as the ratio between the fiber volume and the yarn volume, was equal to $v_f = 0.6$, whereas it varied in the case of warp yarns that were impregnated by the resin using a lamination process. The obtained average peak force F_f, tensile strength σ_f, and elastic modulus E_f, along with the associated coefficient of variation (CoV), are provided in Table 1. The results show that the elastic modulus is consistent among the two types of specimen, although it slightly decreased in the case of the warp yarns since the sub-yarns were twisted and the fibers were not perfectly aligned with the direction of the load. For the same reason, the average tensile strength attained by the warp yarns (σ_f = 817 MPa) was lower than that attained by the weft yarns (σ_f = 1001 MPa). These values show the importance of the epoxy resin impregnation, which promoted the stress redistribution between the fiber filaments allowing for attaining high values of tensile strength [24]. In fact, tests of bare (i.e. not impregnated with the resin) fiber bundles of the same glass fibers reported in [20] provided an average tensile strength of only 581 MPa.

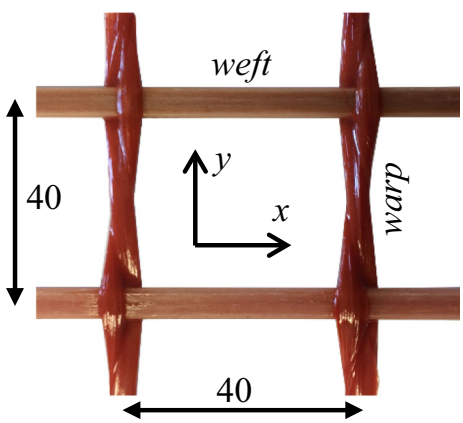

Fig. 1 Glass composite grid (dimensions in mm)

The test conducted showed that the pultruded weft yarns (x-direction) provided a higher tensile strength than the laminated warp yarns (y-direction) due to their different geometry. However, the elastic moduli in weft and warp direction were similar, which indicates that the behavior of the grid will be similar whether the force is applied in the weft or warp direction. The load-carrying capacity contribution of the yarns orthogonal to the applied force direction depends on the grid joint mechanical properties, which are studied in Sect. 3.

2.2 Mortar

The mortar employed in the CRM system included natural hydraulic lime NHL 5 and metakaolin without the addition of cement [25]. Mortars prisms were cast from the same batch used to cast the composite strips (see Sect. 4). Each batch comprised 3 kg of mortars and 0.6 L of water. The specimens were cured at a temperature of 23 ± 2 °C and RH = 0.5 for 28 days before being tested. The average flexural strength f_{mf} = 3.20 MPa of the mortar was obtained by three-point bending tests of three 40 × 40 × 160 mm mortar prisms according to EN 1015-11 [26]. The two portions of the prism obtained after the three-point bending test were tested in compression to obtain the mortar average compressive strength f_{mc} = 8.20 MPa [26]. The values of f_{mf} and f_{mc} were consistent with those previously obtained by the authors for the same mortar cast in a different batch [27]. According to the size-dependent approach provided by Model Code 2010 [28], the tensile strength f_{mt} of the matrix is equal to approximately $0.5f_{mf}$, which provided f_{mt} = 1.60 MPa.

3 Shear strength of grid joints

The fiber grid used in the CRM system is characterized by relatively rigid connections (joints) between weft and warp yarns resulting from the resin impregnation and the leno weave technique adopted. These connections provide the grid geometric stability during

Table 1 Mechanical properties of bare composite grid yarns

Specimen	Number of tests	A_f (mm^2)	F_f (kN) (CoV)	σ_f (MPa) (CoV)	E_f (GPa) (CoV)
Weft (x)	7	5.97	5.98 (11.08%)	1001 (11.08%)	69.91 (2.82%)
Warp (y)	7	5.71	4.66 (7.71%)	817 (7.71%)	66.30 (9.79%)

transportation and installation. Moreover, when a load aligned with one of the directions of the yarns is applied to the CRM, the yarns orthogonal to the applied load direction may provide their contribution to the system load-carrying capacity due to the presence of the grid joints. The shear strength of the joints is of fundamental importance when the glass grid is fixed to the support using only anchorages, without being embedded within the mortar, as in the case of applications to prevent intrados crumbling hazards [29].

To verify the stability of the grid joints and measure the maximum force that can be borne by a single joint, grid cruciform specimens, without the presence of the mortar, were subjected to shear tests. The results obtained provide information only on the behavior of the grid joint and not on the CRM system. The actual behavior of the system may be investigated with a tensile test of the CRM, as described in Sect. 4.

In order to measure the shear strength of the grid joints in weft and warp direction, 10 experimental tests were performed following the indications reported in EN ISO 15630-2 [30], even if this procedure is indicated for steel welded fabrics. The end of the pulling single yarn (either a weft or a warp yarn) was clamped in the machine wedges. The yarn perpendicular to the clamped one, i.e. the crossing yarn, was inserted within a rigid holder, connected to the machine, and firmly tightened using jaws (see Fig. 2a). The tests were conducted by monotonically increasing the displacement δ of the machine actuator at a constant rate of 0.017 mm/s, while the applied load P was registered by a load cell. The specimens were named according to the notation J_G_O_N, where J = joint shear test, G = glass fiber, O indicates the orientation of the grid (X = x-direction, i.e. weft yarn pulled, Y = y-direction, i.e. warp yarn pulled, see Fig. 2), and N is the specimen number. The P–δ curves obtained are shown in Fig. 3. When the weft yarn was pulled (specimens in series J_G_X), the applied load increased linearly up to the sudden shear failure of one of the two crossing twisted sub-yarns comprising the warp yarn. With increasing the displacement δ, the specimen carried a certain applied load until the remaining sub-yarn eventually failed (Fig. 3a). A photo of the shear failure of specimen J_G_X_1 is reported in Fig. 2a. When the warp yarn was pulled (specimens in series J_G_Y), P initially increased linearly (Fig. 3b). With increasing δ, the weft crossing yarn tended to open the two twisted sub-yarns, which determined the non-linear behavior of the P–δ curves. The specimens eventually failed due to the shear failure of the weft yarn (Fig. 2b).

The maximum applied load P^* and corresponding stress σ^*, i.e. the joint shear strength, are reported in Table 2 for each specimen, along with the average value and coefficient of variation obtained by all specimens in x- and y-direction. When the weft yarn was pulled, the joint provided an average maximum stress in the pulling yarn of 183 MPa (P^* = 1.09 kN), whereas a maximum stress in the pulling yarn of 256 MPa (P^* = 1.46 kN) was provided when the warp yarn was pulled.

The measures of the joint shear strength confirmed that weft and warp yarns may concur to the load-carrying capacity of the system even when the applied load is aligned with one of the yarn directions. The shear strengths obtained can be used to estimate the load-carrying capacity of the grid when it is applied using only anchors, without being embedded within the mortar [29]. Furthermore, they can be useful to accurately model the interaction between weft and warp yarns when the grid is embedded within the mortar, i.e. when the CRM system is applied.

4 Tensile properties of the CRM system

The tensile behavior of inorganic-matrix composites is influenced by several parameters, which include the test set-up and procedure. Different test set-ups were proposed in the literature [31–35] and some of them

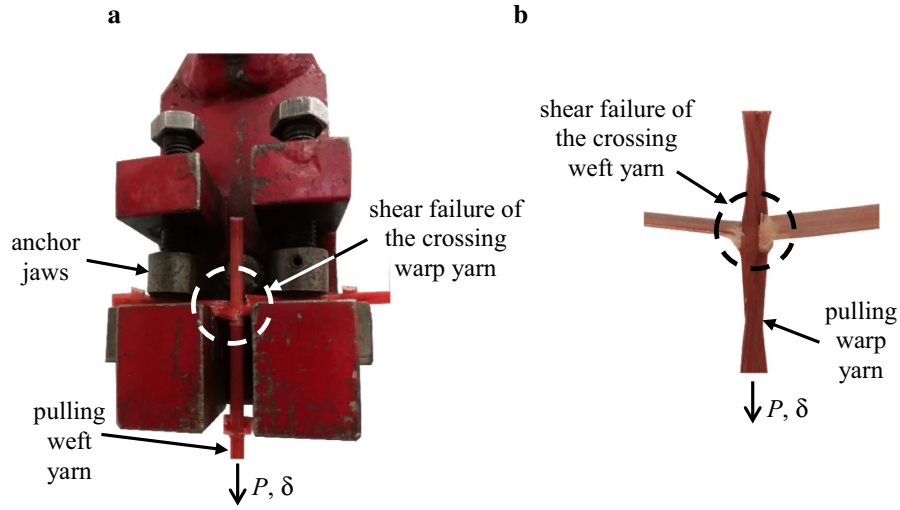

Fig. 2 Shear test on grid joints: **a** test set-up (specimen J_G_X_1, pulling weft); **b** failure of specimen J_G_Y_2 (pulling warp)

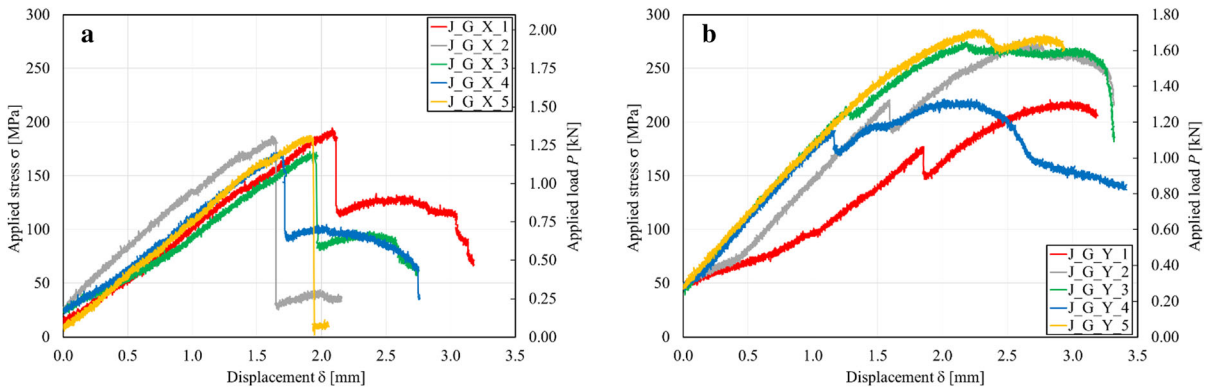

Fig. 3 Load responses of joint shear tests in **a** weft and **b** warp direction

Table 2 Results of the shear tests on the grid joints

Specimen	P^* (kN)	σ^* (MPa)	Specimen	P^* (kN)	σ^* (MPa)
J_G_X_1	1.16	195	J_G_Y_1	1.26	221
J_G_X_2	1.12	187	J_G_Y_2	1.58	276
J_G_X_3	1.03	173	J_G_Y_3	1.57	275
J_G_X_4	1.03	173	J_G_Y_4	1.26	221
J_G_X_5	1.12	188	J_G_Y_5	1.63	286
Average	1.09	183	Average	1.46	256
CoV (%)	5.36		CoV (%)	12.51	

were adopted by current acceptance criteria and design guidelines for externally bonded FRCM composites. According to the Italian acceptance criteria [36], the tensile properties of the inorganic-matrix composite shall be obtained using the clamping-grip tensile test. In this case, the ends of rectangular inorganic-matrix composite coupons are directly clamped by the machine wedges and tensile rupture of the embedded fibers should occur [37]. The U.S. acceptance criteria [38] indicate the use of clevis-grip tests to obtain the tensile acceptance parameters of FRCM and steel reinforced grout (SRG) composites. In the clevis-grip test, metallic plates are bonded to the inorganic-matrix composite coupon ends and are used to transfer the

load from the machine to the specimen through clevis-type joints [34]. These two test set-ups generally provide significantly different results, although they can be both modelled using simple analytical approaches provided that the fiber-matrix bond behavior is known [39].

In this paper, the tensile properties of the glass CRM system were investigated using both the clamping- and clevis-grip test set-up to obtain an insight on the interaction between the grid and the matrix when the CRM is subjected to tensile stress. Two series of 10 specimens were tested using the clamping- and clevis-grip methods, respectively. In each series, 5 specimens had longitudinal weft yarns, i.e. aligned with the applied load direction, and 5 specimens had longitudinal warp yarns. Specimens were named according to the notation TC_G_L_W_O_N, where T = tensile test, C(if present) = clevis-grip set-up (the absence of C indicates a clamping-grip test), G = glass fiber, L = specimen length (in mm), W = specimen width (in mm), O indicates the orientation of the grid (X = *x*-direction, i.e. longitudinal weft yarns, Y = *y*-direction, i.e. longitudinal warp yarns, see Fig. 2), and N is the specimen number. All tests were performed by applying an initial load of approximately 0.1 kN to accommodate the specimen irregularities and check that all instruments were measuring correctly. For this reason, the load responses provided do no start exactly at the origin.

4.1 CRM clamping-grip tensile tests

Rectangular CRM coupons were fabricated following the indications of the Italian acceptance criteria for inorganic-matrix composites [36]. Accordingly, the specimens had a thickness of 10 mm and length of 400 mm. Each specimen included 2 longitudinal yarns and had a width of 60 mm. Although the Italian acceptance criteria recommend a specimen width that is a multiple of the reinforcing mesh space, which would have resulted in a specimen width equal to 80 mm for 2 embedded longitudinal yarns, the width considered in this paper was limited to 60 mm due to the geometry of the clamping wedges. Therefore, the mortar at the lateral edges of the specimens had a width of 10 mm (instead of the recommended 20 mm), which might have affected the specimen response, as discussed below.

A sketch of the test set-up is provided in Fig. 4a. The specimens were equipped with GFRP tabs bonded to the coupon ends to promote an even distribution of the clamping pressure and avoid mortar failure within the wedges. The specimen ends were then directly clamped by hydraulic wedges and the test was carried out by monotonically increasing the end-displacement at a constant rate of 0.0034 mm/s. An extensometer with a gauge length of 200 mm was applied to the central part of the specimen to measure the axial strain ε (Fig. 4b). The extensometer gauge length was determined to capture the majority of the possible matrix cracks. Nevertheless, some cracks occurred close to the wedges also due to stress concentration induced by the clamping pressure (Fig. 4b) and could not be captured by the extensometer. The occurrence of cracks outside the instrument gauge length is well-known in clamping-grip tensile testing of inorganic-matrix composites and may affect the specimen deformability measured [37]. However, the load response obtained can be studied to investigate if the presence of cracks outside the instrument gauge length significantly affects the results [12].

The applied stress σ-axial strain ε curves obtained are shown in Fig. 5a and b for specimens with longitudinal weft and warp yarns, respectively, where σ was computed by dividing the applied load P by the cross-sectional area of the fibers (Table 1). The specimens did not show the tri-linear behavior usually observed in FRCM composites, which is characterized by an initial linear branch (first stage) that ends with the first matrix cracking, a crack development stage (second stage), and a final fully cracked stage where the specimen load-carrying capacity is mainly provided by the embedded textile [37]. In the CRM coupons studied, the first (uncracked) stage was not clearly visible and only specimens of series T_G_400_60_X showed some drops of the applied stress due to the opening of matrix cracks, which are associated with the crack-development stage (i.e. second stage) of the tri-linear response. However, matrix cracks orthogonal to the applied load direction occurred in all specimens (Fig. 4b). The matrix cracking was induced by the reduction of the matrix cross-sectional area at cross-sections where transversal yarns and yarn joints were located. Therefore, matrix cracks were spaced at a distance of approximately 40 mm, which coincides with the grid spacing (see Sect. 2.1).

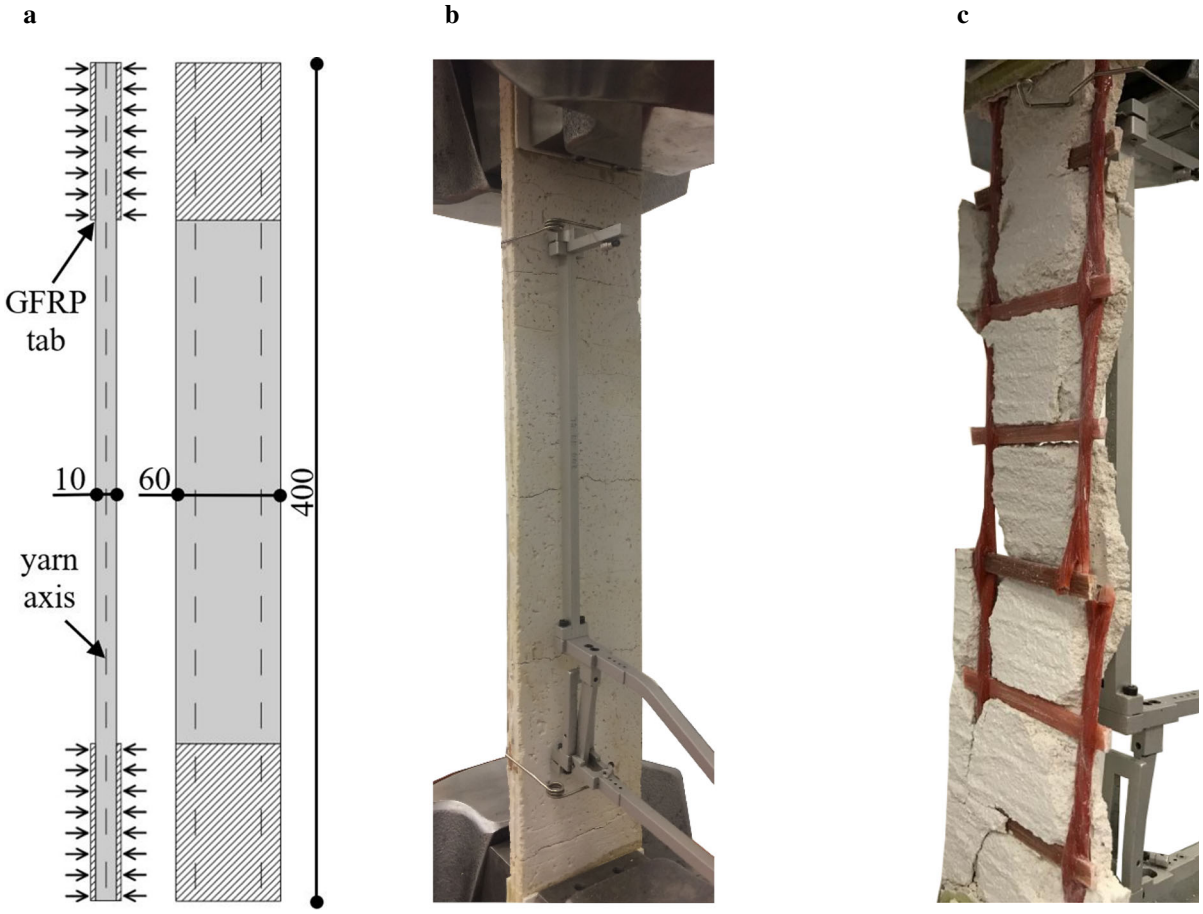

Fig. 4 **a** Sketch of a CRM coupon subjected to the clamping-grip test (dimensions in mm). Specimen T_G_400_60_Y_1 **b** during and **c** at completion of the clamping-grip test

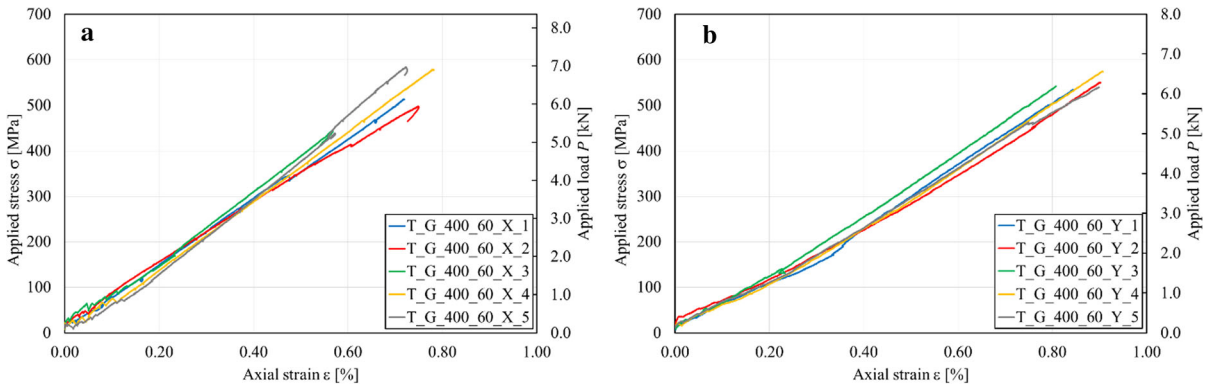

Fig. 5 Clamping-grip tensile tests of CRM coupons in **a** weft and **b** warp direction

The absence of the first and second stages is attributed to the use of a relatively weak matrix and a stiff grid. The impregnation of the glass fibers with the epoxy resin, which plays the key role in the grid stiffness and also generally improves the grid behavior by promoting the stress-transfer among the fiber

filaments in the yarn [40], and the presence of transversal yarns firmly connected to the longitudinal yarns promoted the contribution of the grid to the specimen load-carrying capacity from the initial phases of the test. When non-rigid textiles are employed, as usually occurs in FRCM composites, the fibers provide only a limited contribution to the specimen load-carrying capacity until the occurrence of matrix cracking [12]. A limited extent of the uncracked stage was observed also in clamping-grip tests of steel reinforced grout (SRG) composites [12, 41], which confirms the role of the reinforcement stiffness in the initial phases of the test.

All specimens showed an approximately linear stress–strain behavior after the initial matrix cracking. Assuming that the matrix tension stiffening effect provides a limited contribution to the applied stress, the slope of the linear portion of the σ–ε curves (i.e. fully cracked stage or third stage [12]) should be associated with the longitudinal yarn elastic modulus E_f. In this paper, the slope E_3 of the third stage was computed by linear regression of the σ–ε curves between $0.6\sigma^*$ and $0.9\sigma^*$, where σ^* is the maximum stress attained by the specimen. E_3 computed for each specimen is reported in Table 3 along with the corresponding average value and CoV for each series of specimens. The average values of E_3 is similar to that of bare grid yarns, which confirms that the grid is mainly responsible for the CRM σ–ε curve slope during the third stage, although the matrix and the transversal yarns slightly contributed to the applied load. These results also confirm that the occurrence of matrix cracks outside the extensometer gauge length did not strongly affect the deformability measured.

All specimens failed due to rupture of one of the two longitudinal grid yarns, which was associated with spalling of the matrix (Fig. 4c). The maximum applied load P^*, maximum stress σ^*, and corresponding strain ε^* are provided in Table 3. Due to the rupture of only one longitudinal yarn, the average tensile strengths obtained by CRM coupons were significantly lower than those obtained by tensile tests of bare grid yarns (Table 1). For the same reason, the average maximum applied load $P^* = 6.26$ kN provided by weft CRM coupons was only slightly higher than that of single weft bare grid yarns ($F_f = 5.98$ kN, Table 1), which suggests an uneven distribution of the applied load among the 2 longitudinal yarns. However, the values of E_3 computed, which are similar to E_f, showed that both yarns contributed to bear the load applied to the specimen until $0.9P^*$. Therefore, the rupture of a single yarn should be attributed to the presence of stress concentrations due to the load redistribution.

Warp CRM coupons provided an average maximum applied load $P^* = 6.26$ kN, which is approximately 34% higher than that of single warp bare grid yarns ($F_f = 4.66$ kN, Table 1). This result indicates that a more even load redistribution was attained among the 2 longitudinal yarns in warp CRM coupons than in weft CRM coupons. Since the mortar redistributes the applied load among the yarns, the limited width of the mortar at the specimen lateral edges may have affected the measured coupon load-carrying capacity. Therefore, P^* and σ^* values higher than those reported in Table 3 might be obtained with specimens with a width multiple of the yarn spacing.

The results obtained showed that clamping-grip tensile tests provided tensile strength lower than the tensile strength of bare yarns due to the non-

Table 3 Results the of clamping-grip tests

Specimen	P^* (kN)	σ^* (MPa)	ε^* (%)	E_3 (MPa)	Specimen	P^* (kN)	σ^* (MPa)	ε^* (%)	E_3 (MPa)
T_G_400_60_X_1	6.13	513	0.72	65,800	T_G_400_60_Y_1	6.10	534	0.84	67,810
T_G_400_60_X_2	5.95	498	0.75	57,920	T_G_400_60_Y_2	6.28	550	0.90	67,080
T_G_400_60_X_3	5.31	445	0.57	78,580	T_G_400_60_Y_3	6.19	542	0.81	71,320
T_G_400_60_X_4	6.92	579	0.78	77,480	T_G_400_60_Y_4	6.56	574	0.91	71,550
T_G_400_60_X_5	6.97	584	0.72	99,410	T_G_400_60_Y_5	6.16	539	0.90	63,090
Average	6.26	524	0.71	75,830	Average	6.26	548	0.87	68,170
CoV (%)	11.15		11.60	20.72	CoV (%)	2.86		5.06	5.10

contemporary failure of the two longitudinal embedded yarns. However, the slope of the applied stress-axial strain curves of fully cracked coupons, E_3, was similar to the elastic modulus of bare yarns E_f, which confirms that both yarns contributed to bear the CRM coupon applied load up to $0.9P^*$.

4.2 CRM clevis-grip tensile tests

Two series of rectangular CRM coupons were cast according to the U.S. acceptance criteria AC434 for inorganic-matrix composites [38]. The coupons had the same thickness (i.e. 10 mm) and width (i.e. 60 mm) of those used for the clamping-grip tests, whereas the length was increased to 600 mm. The specimen length was determined in order to maximize the steel plate bonded length up to the maximum value that could be fitted within the testing machine, which was equal to 170 mm (Fig. 6a). The steel plates were bonded to the specimens using an epoxy resin and were connected with a through-pin and a clevis-type joint to the testing machine (Fig. 6a). The tests were conducted by monotonically increasing the machine displacement at a constant rate of 0.0034 mm/s. The specimen axial strain ε was measured using an extensometer with a gauge length of 100 mm mounted to the central part of the specimen (Fig. 6b) and two linear variable displacement transducers (LVDTs) attached to one of the steel plate on one side of the specimen and reacting off of an L-shaped steel plate attached to the opposite steel plate (Fig. 6b). The average of the displacements measured by the two LVDTs was divided by the initial distance between the LVDT support and the L-shaped plate (approximately equal to 260 mm) to compute the axial strain ε. The extensometer adopted complies with the indication of AC434 [38], which recommends the use of an extensometer with a minimum gauge length of

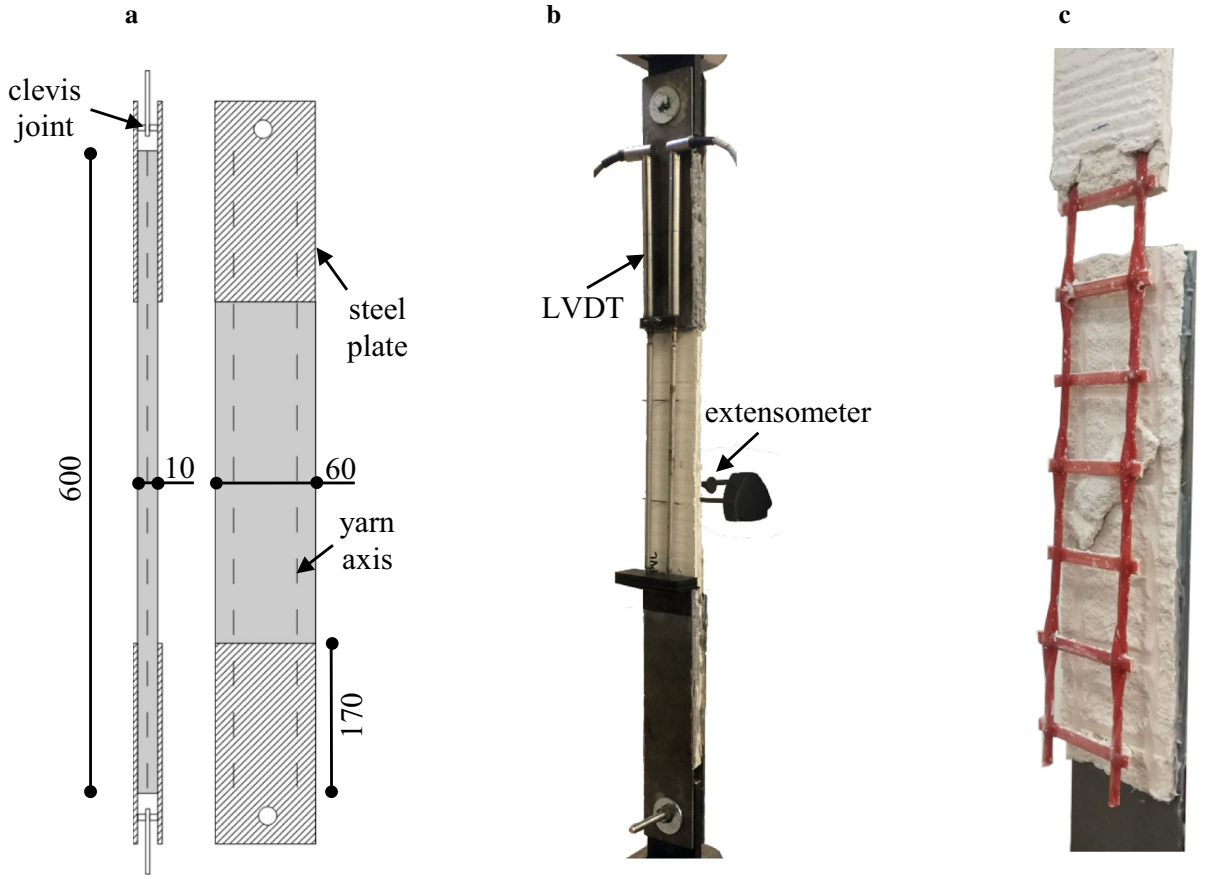

Fig. 6 **a** Sketch of a CRM coupon subjected to the clevis-grip test (dimensions in mm). Specimen TC_G_600_60_Y_1 **b** during and **c** at completion of the clevis-grip test

50 mm able to include at least one transversal matrix crack.

The applied stress σ-axial strain ε curves obtained are shown in Fig. 7a and b for specimens with longitudinal weft and warp yarns, respectively, where σ was computed by dividing the applied load P by the cross-sectional area of the fibers (Table 1) and ε was obtained by the LVDT measurements. As in the clamping-grip tests, the initial uncracked stage was not clearly recognizable except for specimens TC_G_600_60_X_2, TC_G_600_60_Y_2, and TC_G_600_60_Y_4, for which the slope of the σ–ε curve started to decrease at approximately 65 MPa, which was associated to an applied load approximately equal to $P = 0.7$ kN. This applied load corresponds to a stress in the matrix of approximately 1.30 MPa, which is close to the matrix tensile strength $f_{mt} = 1.60$ MPa computed according to the indication of Model Code 2010 [28] (see Sect. 2). The absence of a clearly-recognizable uncracked stage for most of the specimens was attributed to the contribution of the grid from the initial phases of the test, as observed for clamping-grip tests (Sect. 4.1).

The first matrix cracks occurred at the end of the bonded steel plates, as expected in the clevis-grip set-up [39]. After the opening of these cracks, increasing the machine displacement, the applied stress increased and further cracks appeared in the matrix, as shown by the sudden load drops of the σ–ε curves in Fig. 7. The average slope of this cracked stage, which represents the tensile modulus of elasticity of the cracked specimen E_2 according to AC434 [38], was computed by linear regression of the σ–ε curves between $0.6\sigma^*$ and $0.9\sigma^*$, where σ^* is the maximum stress attained by the specimen. The average values of E_2 obtained for weft and warp yarns (Table 4) were lower than the elastic modulus of the bare yarns. This difference is well-known and is caused by slippage of the grid with respect to the matrix in clevis-grip tests [42].

Failure of the specimens occurred due to the sudden matrix interlaminar failure, i.e. splitting along the grid plane [43], between the bonded steel plates (Fig. 6c) without rupture of the longitudinal or transversal yarns. Therefore, the tensile capacity of the grid could not be fully exploited, which entailed for average tensile strength values (Table 4) significantly lower than those obtained for the bare yarns in x- and y-direction (Table 1). Furthermore, the extensive cracking of the matrix led to a large variation of the results, as shown by the coefficient of variation of the maximum applied load P^*, maximum stress σ^*, and corresponding strain ε^* (Table 4).

Figure 8 shows the load responses of two representative specimens in weft and warp direction, namely specimen TC_600_60_X_5 and TC_600_60_Y_3. In Fig. 8, the axial strain of curves named *LVDTs* was obtained from the LVDT measurements, whereas that of curves named *Extensometer* was obtained directly from the extensometer measurements. The extensometer provided a strain generally lower than that obtained by the LVDTs for the same applied stress. The LVDTs measured the relative displacement between the steel plates bonded to the specimen and were able to catch the opening of all matrix cracks. The extensometer, which was applied to the specimen central part, did not capture the opening of the first cracks at the end of the bonded steel plates and of possible other cracks occurring out

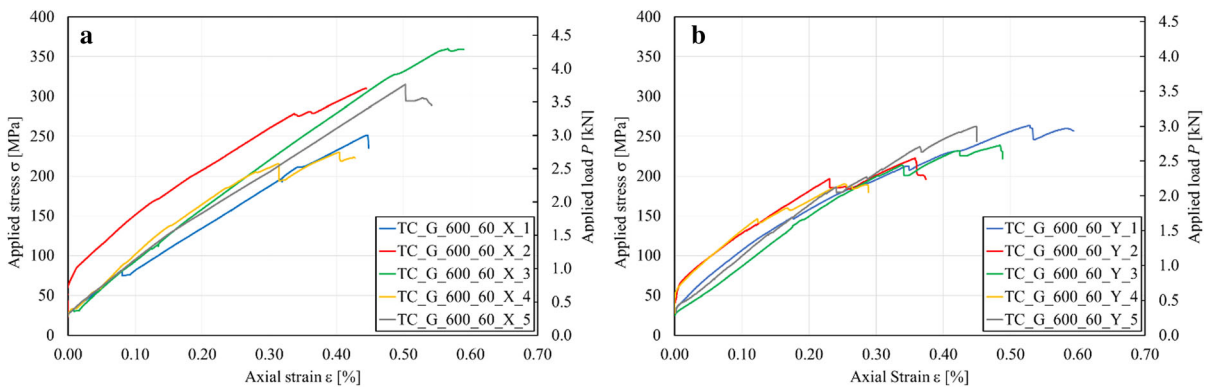

Fig. 7 Clevis-grip tensile tests of CRM coupons in **a** weft and **b** warp direction

Table 4 Results the of clevis-grip tests

Specimen	P^* (kN)	σ^* (MPa)	ε^* (%)	E_2 (MPa)	Specimen	P^* (kN)	σ^* (MPa)	ε^* (%)	E_2 (MPa)
TC_G_600_60_X_1	3.00	252	0.45	49,940	TC_G_600_60_Y_1	3.01	264	0.53	31,760
TC_G_600_60_X_2	3.70	310	0.44	51,210	TC_G_600_60_Y_2	2.54	222	0.36	34,770
TC_G_600_60_X_3	4.30	360	0.57	58,320	TC_G_600_60_Y_3	2.72	238	0.48	39,600
TC_G_600_60_X_4	2.75	230	0.40	53,560	TC_G_600_60_Y_4	2.17	190	0.25	40,400
TC_G_600_60_X_5	3.76	315	0.50	54,130	TC_G_600_60_Y_5	3.02	265	0.60	41,600
Average	3.50	293	0.47	53,430	Average	2.69	236	0.45	37,630
CoV (%)	17.84	17.84	13.30	6.03	CoV (%)	13.26	13.26	31.33	11.12

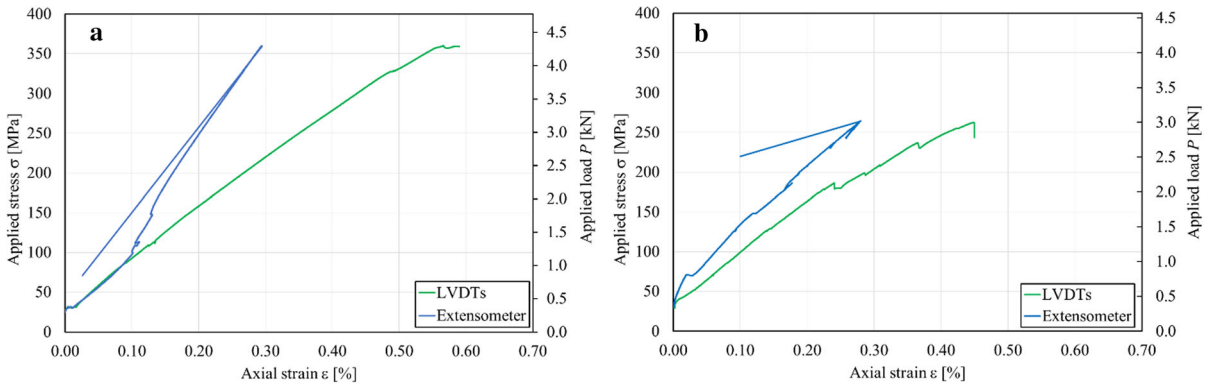

Fig. 8 Load response of specimens **a** TC_600_60_X_5 and **b** TC_600_60_Y_3

of its gauge length. Therefore, the change in slope of the LVDTs and extensometer curves can be employed to identify the openings of matrix cracks that did not cause visible load drops in the σ–ε curves.

Although the axial strains provided by the LVDTs and extensometer were quite similar up to approximately 90 MPa for specimen TC_600_60_X_5 (Fig. 8a), they were different from the beginning of the test for specimen TC_600_60_Y_3 (Fig. 8b). This indicates that significant matrix-grid slips occurred from the beginning of the test in specimen TC_600_60_Y_3. Before the occurrence of the first matrix cracks, these slips are higher between the bonded steel plates than in the central part of the specimen [39], which explains the difference between the LVDTs and extensometer observed in Fig. 8b.

After the tensile strength was attained, the axial strain measured by the extensometer suddenly decreased (note that the post-peak behavior is not shown for LVDTs curves). This indicates that failure occurred outside the extensometer gauge length (see Fig. 6c) leading to the recovering of the elastic elongation of the specimen central part since the reinforcing grid did not fail. The use of an extensometer with gauge length equal to 100 mm provided an axial strain ε substantially different from that obtained by the LVDT measurements. These observations point out the importance of the instrument position and gauge length in the measuring of the axial strain in tensile test of inorganic-matrix materials.

The results obtained showed that clevis-grip tensile tests provided a tensile strength and a slope of the applied stress-axial strain curves E_2 of fully-cracked specimens lower than those observed in clamping-grip tests. These differences are due to the different stress-transfer mechanism in the gripping devices that led to a sudden matrix interlaminar failure in clevis-grip tests. Furthermore, the gauge length and measuring points considered to determine the axial strain in clevis-grip tests had a strong influence on the specimen deformability obtained.

4.3 CRM-masonry bond behavior

The effectiveness of the externally bonded reinforcement is strongly related to the bond between the composite and the substrate and, in the case of FRCM composites, to the matrix-fiber bond behavior [37, 41, 44].

The bond behavior of the glass CRM system considered in this work was investigated by means of 11 single-lap direct shear tests on CRM-masonry joints. Eleven masonry walls made by 6 historical bricks and 5 lime-based mortar joints were constructed. The historical bricks were obtained from the demolition of a building built at the beginning of the twentieth-century in the north of Italy and had a nominal width of 325 mm, thickness of 160 mm, and height of 40 mm. The mechanical properties of the bricks can be found in [20]. Mortar joints with thickness varying between 15 and 20 mm depending on the thickness and planarity of the adjacent bricks were constructed to simulate the texture of an historic wall, which resulted in walls with nominal dimensions of 325 mm (width) × 160 mm (thickness) × 330 mm (height). The surface of the walls was only cleaned with sprayed air to remove dust and then wet with water before the application of the CRM system. The CRM bonded length and width were 290 mm and 120 mm, respectively, which allowed for having 3 longitudinal (i.e. aligned with the applied load direction) yarns (Fig. 9). The matrix nominal overall thickness was 10 mm. Outside the bonded area, the grid was not impregnated with mortar. A pull–push configuration was adopted, where the masonry substrate was restrained and the reinforcing grid was pulled [45]. The masonry wall was restrained by a rigid steel frame, whereas two steel plates were epoxy bonded to the end of the bare strip to promote clamping with the machine (Fig. 9a). Two LVDTs were used to measure the relative displacement of the fiber grid just outside the bonded length at the loaded end and the masonry substrate (see call-out in Fig. 9a). The tests were conducted in displacement control by monotonically increasing the machine displacement at a constant rate of 0.0034 mm/s. Specimens were named according to the notation DS_G_L_W_O_N, where DS = direct shear test, G = glass fiber, L = bonded length (in mm), W = bonded width (in mm), O indicates the orientation of the grid (X = *x*-direction, i.e. longitudinal weft yarns, Y = *y*-direction, i.e. longitudinal warp yarns, see Fig. 2), and N is the specimen number.

The applied stress σ-global slip g curves obtained for each specimen, where the stress was computed by dividing the applied load by the cross-sectional area of the longitudinal yarns and the global slip is the average of the measurements of the two LVDTs, are reported

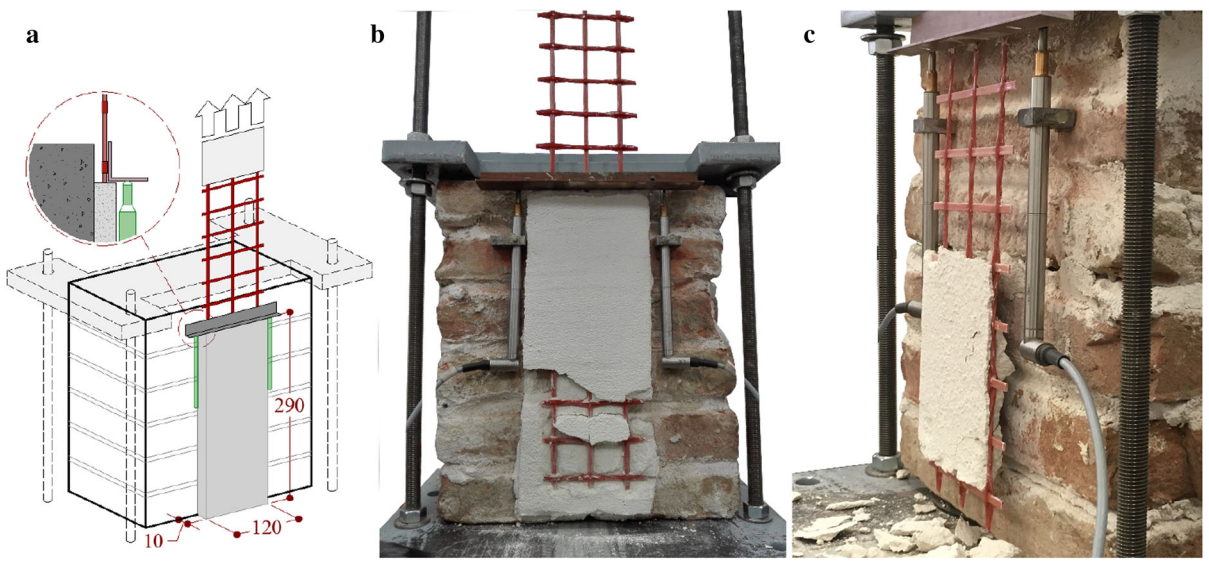

Fig. 9 **a** Sketch of the single-lap direct shear test set-up (dimensions in mm). **b** Specimen DS_G_290_120_X_2 at completion of the test. **c** Failure of specimen DS_G_290_120_Y_3

in Fig. 10. After an initial linear branch, the occurrence of cracks in the matrix determined a non-linear behavior of the σ–g curves. The matrix cracks, which were orthogonal to the direction of the applied load, occurred in the external matrix layer and were caused by the stress concentration induced by the transversal yarns (Fig. 9b). With increasing global slip, the cracks propagated in the matrix toward the masonry support and were responsible for the load drops and sudden increases of g observed in the load responses (Fig. 10). The occurrence of these cracks was previously observed in FRCM composites including stitch-bonded textiles, where the presence of strong connections between longitudinal and transversal yarns determined stress concentration and consequent cracking of the matrix [46].

All specimens eventually failed due to sudden detachment of either the CRM entire strip from the substrate, without damage of the masonry (Fig. 9c), or of the external matrix layer. For specimen DS_290_120_X_1, no matrix cracks occurred due to the premature detachment of the CRM strip, which was attributed to a poor matrix-substrate bond capacity for this specimen. According to the failure mode classification proposed by the Italian acceptance criteria for FRCM composites [36], the failure mode observed included type B (detachment of the CRM strip without damage of the substrate), type C (detachment of the external matrix layer), and type E (slippage of the grid with cracking of the external matrix layer). The failure mode (FM) observed for each specimen is indicated in Table 5.

When one or two layers of textile are employed, failure of FRCM composites generally occurs due to debonding of the fiber from the embedding mortar without cracking of the matrix [8], which is indicated as failure mode D by the Italian acceptance criteria [36]. The occurrence of matrix cracking in the CRM strips can be attributed to the active role of yarns orthogonal to the applied force direction, which is generally not observed in FRCM composites except in those cases where longitudinal and transversal yarns are firmly connected [12]. The detachment of the CRM strip without damage of the substrate can be attributed to poor bond properties at the matrix-substrate interface. Indeed, due to the use of historic bricks, the substrate presented an uneven surface that might have been responsible for the premature detachment of the CRM strip, as observed in specimen DS_G_290_120_X_1.

Table 5 also reports the measured peak load P^*, peak stress σ^*, and corresponding global slip g^* along with the associated average values and coefficient of variation CoV for specimens within the same series. The average peak stress obtained for specimens with warp yarns in the direction of the applied load (DS_G_290_120_Y series) was higher than that of specimens with weft yarns in the direction of the applied load (DS_G_290_120_X series). Since most failure modes involved the matrix-substrate interface (FM type B), the difference in the average peak stresses should be attributed to the randomly distributed matrix-substrate bond properties rather than to the grid-matrix bond behavior, which varies depending on the grid orientation. The matrix cracks and failure modes also affected the global slip g^*, which was particularly scattered for specimens in series DS_G_290_120_X (Table 5).

Since a unique value of CRM bonded length (i.e. 290 mm) was investigated, the peak stress obtained

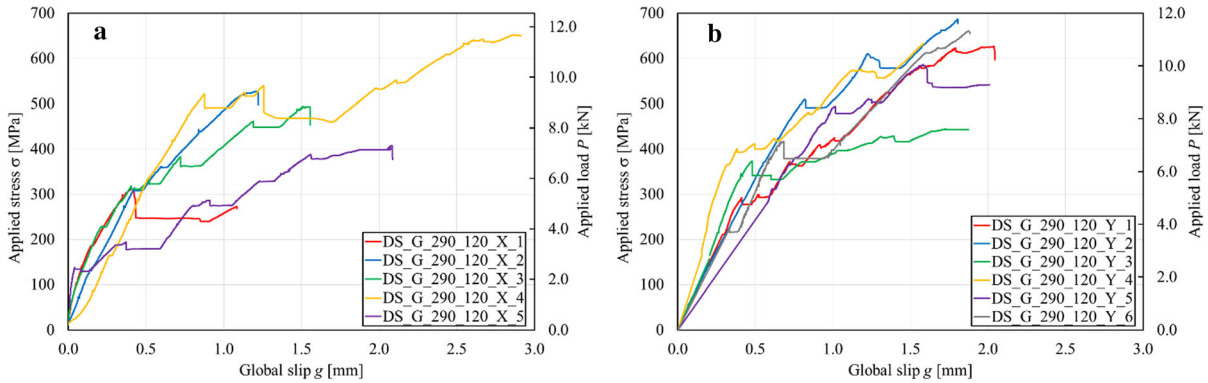

Fig. 10 Applied stress-global slip curves of CRM-masonry direct shear tests in **a** weft and **b** warp direction

Table 5 Direct shear experimental results

Specimen	P^* (kN)	σ^* (MPa)	g^* (mm)	FM	Specimen	P^* (kN)	σ^* (MPa)	g^* (mm)	FM
DS_G_290_120_X_1	5.58	311	0.41	B	DS_G_290_120_Y_1	10.71	626	2.04	E + B
DS_G_290_120_X_2	9.44	527	1.02	E + C	DS_G_290_120_Y_2	11.74	687	1.80	E + B
DS_G_290_120_X_3	8.85	494	1.51	E + B	DS_G_290_120_Y_3	8.30	485	1.76	E + B
DS_G_290_120_X_4	11.67	651	1.26	E	DS_G_290_120_Y_4	11.06	647	1.64	E + B
DS_G_290_120_X_5	7.30	407	2.08	E + B	DS_G_290_120_Y_5	10.03	587	1.59	E + B
					DS_G_290_120_Y_6	11.30	661	1.88	E + B
Average	8.57	478	1.25	–	Average	10.52	615	1.78	–
CoV (%)	26.75		49.00	–	CoV (%)	11.72		9.10	–

FM, failure mode; B, detachment of the CRM strip without damage of the substrate; C, detachment of the external matrix layer; E, slippage of the grid with cracking of the external matrix layer [36]

should not be regarded as the CRM-masonry bond capacity since higher bonded lengths may result in an increase of σ^* [6]. Similarly, the use of matrix thicknesses higher than 10 mm could delay the mortar spalling leading to an increase of the specimen load-carrying capacity.

In clevis-grip tensile tests, when the first matrix cracks have occurred, the grid tends to slip within the embedding matrix along the steel plate bonded length. Therefore, the clevis-grip test can be employed to study the matrix-grid bond behavior of the CRM and the results can be compared to those obtained with corresponding direct shear tests [39]. The peak stresses obtained by direct shear tests (Table 5) were higher than those of clevis-grip tests (Table 4). This difference is mainly attributed to the higher matrix bonded length adopted in direct shear tests (matrix-substrate bonded length) than in clevis-grip tests (matrix-steel plate bonded length). However, the presence of the steel plates bonded to the opposite faces of the specimens in the clevis-grip test may have influenced the matrix-grid stress-transfer mechanism preventing the occurrence of transversal matrix cracks, which were observed in direct shear tests. The results of direct shear tests of CRM-masonry joints showed a good bond behavior in both weft and warp direction, with average peak stresses comparable to the tensile strength values obtained in clamping-grip tensile tests. Failure of the CRM-masonry joints mainly occurred due to cracking of the matrix, which indicates the active role of the transversal yarns in the specimen load-carrying capacity, and detachment of the CRM strip from the substrate. The high exploitation ratios (see next section) obtained encourage further studies of this promising strengthening system. Furthermore, direct shear tests with CRM bonded lengths and matrix thickness higher than those considered may provide an increase of the CRM-masonry joint load-carrying capacity.

5 Remarks on the results obtained

In this section, the average peak loads $\bar{P}^*$ obtained by tensile tests of bare yarns and CRM coupons and by direct shear tests of CRM-masonry joints are compared and discussed. The discussion is made in terms of the average peak load to point out the role of the mortar matrix in redistributing the load among the grid yarns in the CRM system. The exploitation ratio $\eta = \bar{\sigma}^*/\sigma_f$, which expresses the exploitation of the grid tensile capacity and is computed as the ratio between the average peak stress $\bar{\sigma}^*$ obtained by the tests considered and the average tensile strength of the corresponding bare yarns σ_f, is reported in Table 6. The results obtained by the shear test on the grid joints, which are not included in Table 6, should be employed mainly to study the behavior of the grid when it is applied using only anchors, without being embedded in the mortar (see Sect. 3).

The values of $\bar{P}^*$ obtained are compared in Fig. 11. The average peak loads provided by single bare grid yarns ($\bar{P}^* = F_f$ = 5.98 kN and 4.66 kN for weft and warp yarns, respectively, see Table 1) were similar to those obtained by CRM coupons comprising 2 longitudinal yarns tested using the clamping-grip method

Table 6 Exploitation ratios

Type of test	Weft (x) $\bar{\sigma}^*$ (MPa)	Warp (y) $\bar{\sigma}^*$ (MPa)	Weft (x) η (%)	Warp (y) η (%)
Bare yarn tensile test	1001[†]	817[†]	–	–
Clamping-grip tensile test	524	548	52.35	67.07
Clevis-grip tensile test	293	236	29.27	28.89
Direct shear test	478	615	47.75	75.28

[†] $\bar{\sigma}^* = \sigma_f$ for bare yarn tensile tests

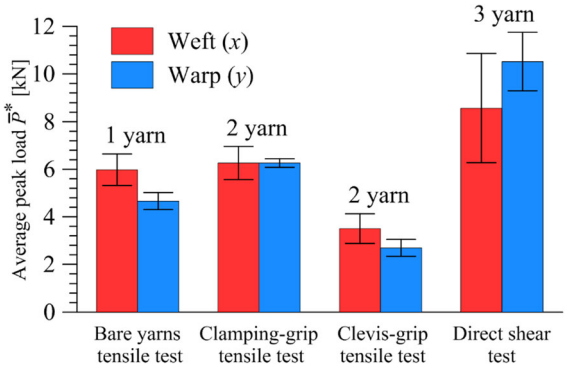

Fig. 11 Average peak force obtained by tensile tests of bare yarns and CRM coupons and by direct shear tests of CRM-masonry joints

($\bar{P}^* = F_f = 6.26$ kN for both longitudinal weft and warp yarns, see Table 2), due to the rupture of a single yarn in CRM coupons (Sects. 4.1 and 4.2). This indicates an uneven stress distribution among the yarns, which is partly attributed to the limited width of mortar at the specimen lateral edges, and to the presence of stress concentrations in CRM coupons that led to rupture of one of the yarns. A more even load distribution can be postulated for CRM coupons with longitudinal warp yarns than with weft yarns, which allowed for a higher exploitation ratio for warp coupons ($\eta = 67.07\%$) than for weft coupons ($\eta = 52.35\%$).

Whereas in clamping-grip tests the wedge pressure helps the load transfer from the machine to the reinforcing grid, in the clevis-grip tensile tests the load is transferred from the mortar matrix to the grid through shear stresses at the matrix-grid interface and through the matrix-grid interlocking allowed by the grid joints [12, 34]. Therefore, the average peak load $\bar{P}^*$ of clevis-grip tensile tests is related to the matrix-grid bond properties and to the matrix capacity to transfer the load among longitudinal and transversal yarns by interlocking. The lime-based mortar employed in this CRM system showed cracks orthogonal and parallel to the applied load direction. The clevis-grip coupons eventually failed due to the opening of a main crack along the grid plane. This behavior led to quite similar, though low, values of the exploitation ratio both for weft ($\eta = 29.27\%$) and warp ($\eta = 28.89\%$) CRM coupons. However, similarly to the case of clamping-grip tests, the limited width of the mortar at the lateral edges of clevis-grip specimens may have influenced the result obtained. Using a width multiple of the grid spacing may result in a better load redistribution among the yarns and consequent higher $\bar{P}^*$ values than in the case of the specimens tested.

In direct shear tests of CRM-masonry joints, the load is applied to the composite by direct clamping the grid (Fig. 9), which transfers the stresses to the substrate through mechanisms similar to those involved in the clevis-grip tensile test [39]. However, the masonry substrate contrasted the opening of matrix cracks, allowing for attaining exploitation ratios similar to those provided by clamping-grip tests. This indicates that an effective stress-transfer occurs among the CRM and the substrate. Supplementary tests with composite bonded lengths higher than 290 mm will clarify if the CRM-substrate stress-transfer mechanism was fully exploited or if the CRM-masonry joint load-carrying capacity could further increase.

6 Conclusions

The goal of this paper was the definition of appropriate experimental tests of composite reinforced mortar (CRM) systems and of their components to obtain the mechanical properties needed to design different CRM strengthening applications. The main mechanical properties of a specific glass CRM system were investigated. The results were discussed pointing out the importance of the parameters obtained, while

indications concerning the set-up and instrumentations of each specific test procedure were provided. The following tests were proposed to reach a complete mechanical characterization of CRM composites that allows for obtaining the main variables needed to design different strengthening applications:

(a) Tensile tests of bare grid yarns, which allowed for obtaining the grid mechanical properties in the two orthogonal directions.
(b) Shear strength tests of grid joints, which provided indications on the grid load-carrying capacity when it is applied using anchors.
(c) Tensile tests of CRM coupons, which provided indications on the mechanical behavior of the CRM when subjected to pure tension. These tests were carried out according to the Italian and U.S. acceptance criteria for inorganic-matrix composites using two alternative clamping systems, each providing different information on the CRM mechanical properties.
(d) Direct shear tests of CRM-substrate joints, which appear essential to assess the CRM-substrate stress-transfer mechanism in both orthogonal yarn directions, showed that failure occurred due to cracking of the matrix and detachment of the CRM strip.

The investigations discussed in this paper confirm that CRM systems represent a promising strengthening solution. Further studies should be performed to formulate shared and reliable acceptance criteria and design procedure for this type of material.

Acknowledgements Open access funding provided by Politecnico di Milano within the CRUI-CARE Agreement. The experimental tests described in this paper were carried out at Laboratorio Prove Materiali of Politecnico di Milano. TCS s.r.l. is gratefully acknowledged for providing the CRM system.

Compliance with ethical standards

Conflict of interest The authors declare that they have no conflict of interest.

References

1. Pantazopoulou SJ, Tastani SP, Thermou GE et al (2016) Background to the European seismic design provisions for retrofitting RC elements using FRP materials. Struct Concr 17:194–219. https://doi.org/10.1002/suco.201500102
2. Lignola GP, Prota A, Manfredi G (2012) Numerical investigation on the influence of FRP retrofit layout and geometry on the in-plane behavior of masonry walls. J Compos Constr 16:712–723. https://doi.org/10.1061/(ASCE)CC.1943-5614.0000297
3. Foraboschi P (2016) Effectiveness of novel methods to increase the FRP-masonry bond capacity. Compos Part B 107:214–232. https://doi.org/10.1016/j.compositesb.2016.09.060
4. Panizza M, Garbin E, Valluzzi MR, Modena C (2015) Experimental study of the bond of FRP applied to natural stones and masonry prisms. Key Eng Mater. https://doi.org/10.4028/www.scientific.net/KEM.624.453
5. De Lorenzis L, Dimitri R, La Tegola A (2007) Reduction of the lateral thrust of masonry arches and vaults with FRP composites. Constr Build Mater 21:1415–1430. https://doi.org/10.1016/j.conbuildmat.2006.07.009
6. Carrara P, Ferretti D, Freddi F (2013) Debonding behavior of ancient masonry elements strengthened with CFRP sheets. Compos Part B 45:800–810. https://doi.org/10.1016/j.compositesb.2012.04.029
7. Ferrari L (2019) First-aid and provisional devices in historical structures with collapse risk after seismic shock. Key Eng Mater 817:301–308. https://doi.org/10.4028/www.scientific.net/KEM.817.301
8. American Concrete Institute (2013) Guide to design and construction of externally bonded fabric-reinforced cementitious matrix (FRCM) systems for repair and strengthening concrete and masonry structures. ACI 549.4R-13. ACI, Farmington Hills
9. Younis A, Ebead U, Shrestha K (2020) Tensile characterization of multi-ply fabric-reinforced cementitious matrix strengthening systems. Struct Concr. https://doi.org/10.1002/suco.201900076
10. Barducci S, Alecci V, De Stefano M et al (2020) Experimental and analytical investigations on bond behavior of basalt-FRCM systems. J Compos Constr 24:04019055. https://doi.org/10.1061/(ASCE)CC.1943-5614.0000985
11. Misseri G, Stipo G, Galassi S, Rovero L (2019) Experimental investigation on the bond behaviour of basalt TRM systems—influence of textile configuration and multi-layer application. In: Key engineering materials/KEM.817.134
12. D'Antino T, Papanicolaou C (2017) Mechanical characterization of textile reinforced inorganic-matrix composites. Compos Part B 127:78–91. https://doi.org/10.1016/j.compositesb.2017.02.034

13. Alecci V, Focacci F, Rovero L et al (2016) Extrados strengthening of brick masonry arches with PBO–FRCM composites: experimental and analytical investigations. Compos Struct 149:184–196. https://doi.org/10.1016/j.compstruct.2016.04.030
14. Sneed LH, Baietti G, Fraioli G, Carloni C (2019) Compressive behavior of brick masonry columns confined with steel-reinforced grout jackets. J Compos Constr 23:04019037. https://doi.org/10.1061/(ASCE)CC.1943-5614.0000963
15. Incerti A, Vasiliu A, Ferracuti B, Mazzotti C (2015) Uniaxial compressive tests on masonry columns confined by FRP and FRCM. In: Proceedings of the 12th international symposium on fiber reinforced polymers for reinforced concrete structures (FRPRCS-12) and the 5th Asia-Pacific conference on fiber reinforced polymers in structures (APFIS-2015) joint conference, Nanjing, China, p 6
16. Borri A, Castori G, Corradi M, Speranzini E (2011) Shear behavior of unreinforced and reinforced masonry panels subjected to in situ diagonal compression tests. Constr Build Mater 25:4403–4414. https://doi.org/10.1016/j.conbuildmat.2011.01.009
17. Koutas LN, Bournas DA (2019) Out-of-plane strengthening of masonry-infilled RC frames with textile-reinforced mortar jackets. J Compos Constr 23:04018079. https://doi.org/10.1061/(ASCE)CC.1943-5614.0000911
18. Gattesco N, Boem I, Dudine A (2015) Diagonal compression tests on masonry walls strengthened with a GFRP mesh reinforced mortar coating. Bull Earthq Eng 13:1703–1726. https://doi.org/10.1007/s10518-014-9684-z
19. Del Zoppo M, Di Ludovico M, Balsamo A, Prota A (2019) In-plane shear capacity of tuff masonry walls with traditional and innovative composite reinforced mortars (CRM). Constr Build Mater 210:289–300. https://doi.org/10.1016/j.conbuildmat.2019.03.133
20. D'Antino T, Carozzi FG, Poggi C (2019) Diagonal shear behavior of historic walls strengthened with composite reinforced mortar (CRM). Mater Struct 52:114. https://doi.org/10.1617/s11527-019-1414-1
21. CSLLPP - Servizio Tecnico Centrale (2019) Linea Guida per la identificazione, la qualificazione ed il controllo di accettazione dei sistemi a rete preformata in materiali compositi fibrorinforzati a matrice polimerica da utilizzarsi per il consolidamento strutturale di costruzioni esistenti con la tecnica dell'intonaco armato CRM (Composite Reinforced Mortar). Rome, Italy
22. TCS Calce (2019) TCS GLASS MR44 technical sheet, July 2019
23. National Research Council (2013) Guide for the design and construction of externally bonded FRP systems for strengthening existing structures. CNR-DT 200/R1. CNR, Rome, Italy
24. D'Antino T, Poggi C (2019) Stress redistribution in glass fibers of G-FRCM composites. Key Eng Mater. https://doi.org/10.4028/www.scientific.net/KEM.817.520
25. TCS Calce (2019) B-STRUCTURA technical sheet, October 2019
26. European Committee for Standardization (1999) Methods of test for mortar for masonry. Determination of flexural and compressive strength of hardened mortar. EN 1015-11:1999. CEN, Brussels
27. Carozzi FG, D'Antino T, Poggi C (2018) In-situ experimental tests on masonry panels strengthened with textile reinforced mortar composites. Proc Struct Int 11:355–362. https://doi.org/10.1016/j.prostr.2018.11.046
28. Federation Internationale du Beton (2013) Fib model code for concrete structures 2010. Ernst & Sohn GmbH & Co, Berlin
29. D'Antino T, Calabrese AS, Poggi C et al (2020) Strengthening of different types of slabs with composite-reinforced mortars (CRM). Build Educ. https://doi.org/10.1007/978-3-030-33687-5_26
30. European Committee for Standardization (2019) Steel for the reinforcement and prestressing of concrete—test methods. Part 2: welded fabric and lattice girders. EN ISO 15630-2:2019. CEN, Brussels
31. Contamine R, Si Larbi A, Hamelin P (2011) Contribution to direct tensile testing of textile reinforced concrete (TRC) composites. Mater Sci Eng A 528:8589–8598. https://doi.org/10.1016/j.msea.2011.08.009
32. Hartig J, Jesse F, Schicktanz K, Häußler-Combe U (2012) Influence of experimental setups on the apparent uniaxial tensile load-bearing capacity of textile reinforced concrete specimens. Mater Struct 45:433–446. https://doi.org/10.1617/s11527-011-9775-0
33. D'Antino T, Papanicolaou C (2018) Comparison between different tensile test set-ups for the mechanical characterization of inorganic-matrix composites. Constr Build Mater 171:140–151. https://doi.org/10.1016/j.conbuildmat.2018.03.041
34. Arboleda D, Carozzi FG, Nanni A, Poggi C (2016) Testing procedures for the uniaxial tensile characterization of fabric-reinforced cementitious matrix composites. J Compos Constr 20:04015063. https://doi.org/10.1061/(ASCE)CC.1943-5614.0000626
35. Donnini J, Chiappini G, Lancioni G, Corinaldesi V (2019) Tensile behaviour of glass FRCM systems with fabrics' overlap: experimental results and numerical modeling. Compos Struct 212:398–411. https://doi.org/10.1016/j.compstruct.2019.01.053
36. CSLLPP - Servizio Tecnico Centrale (2019) Linee guida per la identificazione, la qualificazione ed il controllo di accettazione di compositi fibrorinforzati a matrice inorganica (FRCM) da utilizzarsi per il consolidamento strutturale di costruzioni esistenti. Rome, Italy
37. Carozzi FG, Poggi C (2015) Mechanical properties and debonding strength of Fabric reinforced cementitious matrix (FRCM) systems for masonry strengthening. Compos Part B 70:215–230. https://doi.org/10.1016/j.compositesb.2014.10.056
38. International Code Council Evaluation Service (ICC-ES) (2018) Acceptance criteria for masonry and concrete strengthening using fabric-reinforced cementitious matrix (FRCM) and steel reinforced grout (SRG) composite systems. AC434. Whittier, CA
39. Focacci F, D'Antino T, Carloni C (2019) Analytical modelling of the tensile response of PBO-FRCM composites. In: Proceedings of the twenty-fourth Italian Association of theoretical and applied mechanics convention (AIMETA 2019). Springer, Rome, pp 527–536
40. Dvorkin D, Peled A (2016) Effect of reinforcement with carbon fabrics impregnated with nanoparticles on the tensile

behavior of cement-based composites. Cem Concr Res 85:28–38. https://doi.org/10.1016/j.cemconres.2016.03.008
41. De Santis S, Ceroni F, de Felice G et al (2017) Round robin test on tensile and bond behaviour of steel reinforced grout systems. Compos Part B 127:100–120. https://doi.org/10.1016/j.compositesb.2017.03.052
42. D'Antino T, Carozzi FG, Colombi P, Poggi C (2018) Out-of-plane maximum resisting bending moment of masonry walls strengthened with FRCM composites. Compos Struct 202:881–896. https://doi.org/10.1016/j.compstruct.2018.04.054
43. Carabba L, Santandrea M, Carloni C et al (2017) Steel fiber reinforced geopolymer matrix (S-FRGM) composites applied to reinforced concrete structures for strengthening applications: a preliminary study. Compos Part B 128:83–90. https://doi.org/10.1016/j.compositesb.2017.07.007
44. Ombres L, Mancuso N, Mazzuca S, Verre S (2019) Bond between carbon fabric-reinforced cementitious matrix and masonry substrate. J Mater Civil Eng 31:04018356. https://doi.org/10.1061/(ASCE)MT.1943-5533.0002561
45. Ombres L, Iorfida A, Verre S (2019) FRCM/SRG-masonry joints: experimental investigation and numerical modelling. Key Eng Mater. https://doi.org/10.4028/www.scientific.net/KEM.817.3
46. Mazzucco G, D'Antino T, Pellegrino C, Salomoni V (2018) Three-dimensional finite element modeling of inorganic-matrix composite materials using a mesoscale approach. Compos Part B 143:75–85. https://doi.org/10.1016/j.compositesb.2017.12.057